

# On the Average Mutual Information of MIMO Keyhole Channels with Finite Inputs

Chongjun Ouyang, Yuanwei Liu, Julian Cheng, Ralf R. Müller, and Hongwen Yang

**Abstract**—This letter studies the average mutual information (AMI) of keyhole multiple-input multiple-output (MIMO) systems having finite input signals. At first, the AMI of single-stream transmission is investigated under two cases where the state information at the transmitter (CSIT) is available or not. Then, the derived results are further extended to the case of multi-stream transmission. For the sake of providing more system insights, asymptotic analyses are performed in the regime of high signal-to-noise ratio (SNR), which suggests that the high-SNR AMI converges to some constant with its rate of convergence determined by the diversity order. All the results are validated by numerical simulations and are in excellent agreement.

**Index Terms**—Average mutual information (AMI), finite input, keyhole channel, performance analysis.

## I. INTRODUCTION

Multiple-input multiple-output (MIMO) systems are known to boost the spectral efficiency (SE) performance of wireless channels in contrast to the conventional single-antenna systems. Yet, practical MIMO systems may suffer from severe degradation of the SE due to the degenerate channel phenomena. One of the most typical issues is termed the keyhole effect which may arise in a corridor when the waves are propagated through the same hole [1]–[5]. The existence of this effect was first predicted in theory [1] and then validated by actual measurement [6]. Theoretically, the keyhole effect can reduce the multiplexing gain of a MIMO channel to unity [1], which, thus, models the worst-case propagation environment for MIMO systems from the SE perspective. Generally, the system SE is proportional to the input-output mutual information (MI). Hence, analyzing the MI of keyhole MIMO channels can benchmark the SE performance of multiple-antenna systems.

Motivated by the significance of studying the achievable MI of keyhole MIMO channels, several researchers investigated the average MI (AMI) of keyhole MIMO channels having Gaussian distributed input signals [2]–[5]. Sadly, practical transmit signals are generally taken from finite constellation alphabets, e.g., quadrature amplitude modulation (QAM), rather than Gaussian ones. Moreover, it is worth noting that the AMI achieved by finite-input signals differs from that achieved by

Gaussian signals, especially in the high signal-to-noise (SNR) region [7]. Thus, studying the AMI of keyhole MIMO channels having finite inputs makes important sense. Unfortunately, this problem still remains open as well as unsolved.

To fill this knowledge gap, this letter investigates the AMI of keyhole MIMO channels having finite inputs under Nakagami- $m$  fading. Particularly, we discuss the AMI under both single-stream (SS) and multi-stream (MS) transmission. For a through study, the cases where the state information at the transmitter (CSIT) is available and unavailable are both studied. To glean more system insights, we perform asymptotic analysis to the AMI in the high-SNR region and specify the diversity order of the considered system.

## II. SYSTEM MODEL

In a point-to-point keyhole MIMO channel illustrated in Fig. 1, an  $N_t$ -antenna transmitter (Tx) sends wireless signal to an  $N_r$ -antenna receiver (Rx). The received signal is given as

$$\mathbf{y} = \sqrt{\bar{\gamma}}\mathbf{H}\mathbf{s} + \mathbf{n}, \quad (1)$$

where  $\mathbf{H} \in \mathbb{C}^{N_r \times N_t}$  denotes the channel matrix with  $N_t > 1$  and  $N_r > 1$ ,  $\mathbf{s} \in \mathbb{C}^{N_t \times 1}$  denotes the transmit signal vector with  $\mathbb{E}\{\mathbf{s}^H\mathbf{s}\} = 1$ ,  $\bar{\gamma}$  denotes the transmit SNR, and  $\mathbf{n} \sim \mathcal{CN}(\mathbf{0}, \mathbf{I}_{N_r})$  denotes the additive white Gaussian noise (AWGN). Exploiting the spatial structure of keyhole channels, we have [1]

$$\mathbf{H} = \mathbf{h}_r\mathbf{h}_t^H, \quad (2)$$

where  $\mathbf{h}_r = [\alpha_1 e^{j\phi_1}, \dots, \alpha_{N_r} e^{j\phi_{N_r}}]^T \in \mathbb{C}^{N_r \times 1}$  and  $\mathbf{h}_t = [\beta_1 e^{j\psi_1}, \dots, \beta_{N_t} e^{j\psi_{N_t}}]^T \in \mathbb{C}^{N_t \times 1}$  denote the keyhole-to-Rx and Tx-to-keyhole channel vectors, respectively. Moreover, assume that all the entries in the channel vector  $\mathbf{h}_r$  are independently and identically distributed (i.i.d.). Particularly, the magnitude  $\alpha_i$  ( $\forall i$ ) follows Nakagami- $m$  distribution with its probability density function (PDF) given by  $f_\alpha(x) = \frac{2}{\Gamma(m_r)} m_r^{m_r} x^{2m_r-1} e^{-m_r x^2}$  ( $x > 0$ ), where  $m_r = \frac{1}{\mathbb{E}\{\alpha_i^2\}} \geq 0.5$  indicates the fading severity;  $\Gamma(x) \triangleq \int_0^\infty t^{x-1} e^{-t} dt$  is the gamma function [8, eq. (8.310.1)]; the phase  $\phi_i$  ( $\forall i$ ) is uniformly distributed in  $[0, 2\pi]$ . Likewise, we assume that the Tx-to-keyhole channel undergoes i.i.d. Nakagami- $m$  fading; thus, the PDF of the magnitude  $\beta_i$  ( $\forall i$ ) is given as  $f_\beta(x) = \frac{2}{\Gamma(m_t)} m_t^{m_t} x^{2m_t-1} e^{-m_t x^2}$  ( $x > 0$ ,  $m_t \geq 0.5$ ) and the phase  $\psi_i$  ( $\forall i$ ) is uniformly distributed in  $[0, 2\pi]$ .

## III. SINGLE-STREAM TRANSMISSION

Having introduced the basic model of the keyhole channel, let us move on to discuss the average mutual information

C. Ouyang and H. Yang are with the School of Information and Communication Engineering, Beijing University of Posts and Telecommunications, Beijing, 100876, China (e-mail: {DragonAim, yanghong}@bupt.edu.cn).

Y. Liu is with the School of Electronic Engineering and Computer Science, Queen Mary University of London, London, E1 4NS, U.K. (e-mail: yuanwei.liu@qmul.ac.uk).

J. Cheng is with the School of Engineering, The University of British Columbia, Kelowna, BC V1V 1V7, Canada (email: julian.cheng@ubc.ca).

R. R. Müller are with the Institute for Digital Communications, Friedrich-Alexander-Universität Erlangen-Nürnberg, 91058, Erlangen, Germany (e-mail: ralf.r.mueller@fau.de).

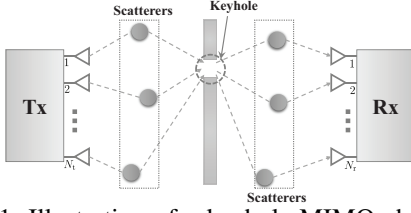


Fig. 1: Illustration of a keyhole MIMO channel.

of this channel achieved by finite input signals. We first consider the scenario of single-stream transmission where the transmitted signal vector,  $\mathbf{s}$ , in (1) satisfies

$$\mathbf{s} = \mathbf{w}x. \quad (3)$$

The terms appearing in (3),  $\mathbf{w} \in \mathbb{C}^{N_t \times 1}$  denotes the precoding vector satisfying  $\|\mathbf{w}\|^2 = 1$  and  $x \in \mathbb{C}$  denotes the transmitted symbol satisfying  $\mathbb{E}\{|x|^2\} = 1$ . Furthermore, we assume that  $x$  is taken from a finite constellation alphabet  $\mathcal{X}$  consisting of  $M$  points,  $\{\mathbf{x}_i\}_{i=1}^M$ , with equal probabilities. Before analyzing the average mutual information of the fading channel, we first discuss the MI of a scalar Gaussian channel:

$$Y = \sqrt{\gamma}X + Z, \quad (4)$$

where  $Z \sim \mathcal{CN}(0, 1)$  denotes the AWGN,  $X$  is taken from the equiprobable constellation alphabet  $\mathcal{X}$ , and  $\gamma$  is the SNR. The MI (in 'bits/s/Hz') of this channel is given by [7]

$$I_M^{\mathcal{X}}(\gamma) = \log_2 M - \frac{1}{M\pi} \sum_{j=1}^M \int_{\mathbb{C}} e^{-|u - \sqrt{\gamma}x_j|^2} \times \log_2 \left( \sum_{k=1}^M e^{|u - \sqrt{\gamma}x_j|^2 - |u - \sqrt{\gamma}x_k|^2} \right) du. \quad (5)$$

Taking (3) and (5) together, the AMI achieved by single-stream transmission (SS-AMI) can be written as  $\mathcal{I}_M^{\mathcal{X}} = \mathbb{E}_{\mathbf{H}} \left\{ I_M^{\mathcal{X}}(\bar{\gamma} \|\mathbf{h}_r\|^2 |\mathbf{h}_t^H \mathbf{w}|^2) \right\}$ . It is worth mentioning that the AMI,  $\mathcal{I}_M^{\mathcal{X}}$ , depends on the precoding vector  $\mathbf{w}$ . In the sequel, we will analyze the AMI based on the availability of CSIT.

#### A. Without CSIT

When the transmitter has no access to the CSI, the precoding vector is given by  $\mathbf{w} = \frac{1}{\sqrt{N_t}} \mathbf{1}$ . In this case, we have  $\mathcal{I}_M^{\mathcal{X}} = \mathbb{E} \left\{ I_M^{\mathcal{X}}(S_1 \bar{\gamma} / N_t) \right\}$ , where  $S_1 = \|\mathbf{h}_r\|^2 |\mathbf{h}_t^H \mathbf{1}|^2 = \left( \sum_{i=1}^{N_t} \alpha_i^2 \right) \left| \sum_{i=1}^{N_t} \beta_i e^{j\psi_i} \right|^2$ .

1) *Channel Statistics*: To characterize the AMI, it is necessary to derive the PDF of  $S_1$ . For brevity, assume that  $m_t$  takes integers, and the following two lemmas can be found.

**Lemma 1.** The PDF of  $G = \left| \sum_{i=1}^{N_t} \beta_i e^{j\psi_i} \right|^2$  is given by

$$f_G(x) = \mathcal{G} \left\langle e^{-\frac{x}{4U_{N_t}}} x^j (4U_{N_t})^{-j-1} \right\rangle. \quad (6)$$

The terms appearing in (6), the operator  $\mathcal{G} \langle \cdot \rangle$  is defined as

$$\mathcal{G} \langle \mathcal{Y} \rangle \triangleq \sum_{i_1=0}^{m_t-1} \cdots \sum_{i_{N_t}=0}^{m_t-1} \sum_{j=0}^{S_{N_t}} \frac{(-S_{N_t})_j S_{N_t}! Y_{N_t} \mathcal{Y}}{\prod_{k=1}^{N_t} \left( \frac{(i_k!)^2}{(1-m_t)_{i_k}} \right) (j!)^2 U_{N_t}^{S_{N_t}}}, \quad (7)$$

where  $\mathcal{Y}$  being a mathematical expression and  $\mathcal{G} \langle \mathcal{Y} \rangle$  means replacement of the  $\mathcal{Y}$  in (7) with this expression. Besides,

$S_{N_t} = \sum_{k=1}^{N_t} i_k$ ,  $Y_{N_t} = \prod_{k=1}^{N_t} \left( \frac{1}{4m_t} \right)^{i_k}$ ,  $U_{N_t} = \sum_{k=1}^{N_t} \frac{1}{4m_t}$ , and  $(z)_n \triangleq \frac{\Gamma(z+n)}{\Gamma(z)}$  is the Pochhammer's symbol [9, eq. (5.2.5)] with  $(-z)_n = (-1)^n (z - n + 1)_n$ .

*Proof:* Please refer to [10] for more details. ■

**Lemma 2.** The PDF of  $S_1$  is given by

$$f_{S_1}(x) = \mathcal{G} \left\langle \frac{2}{\Gamma(N_r m_r)} \left( \frac{m_r}{4U_{N_t}} \right)^{\frac{N_r m_r + j + 1}{2}} \times x^{\frac{N_r m_r + j - 1}{2}} K_{N_r m_r - j - 1} \left( 2\sqrt{\frac{m_r x}{4U_{N_t}}} \right) \right\rangle, \quad (8)$$

where  $K_\nu(\cdot)$  is the  $\nu$ -th order modified Bessel function of the second kind [8, eq. (8.446)].

*Proof:* Since  $\{\alpha_i\}_{i=1}^{N_t}$  are  $N_t$  i.i.d. Nakagami- $m$  variables, the PDF of  $F = \|\mathbf{h}_r\|^2$  can be written as  $f_F(x) = \frac{1}{\Gamma(N_r m_r)} m_r^{N_r m_r} x^{N_r m_r - 1} e^{-m_r x}$ . Exploiting the statistical independency of  $G$  and  $F$ , we can consequently calculate the PDF of the product  $S_1 = GF$  as  $f_{S_1}(x) = \int_0^\infty f_G\left(\frac{x}{y}\right) f_F(y) \frac{1}{y} dy$ . Making use of the integral identify [8, eq. (3.471.9)], we finally get the desired PDF shown in (8). ■

2) *Explicit Analysis*: Using Lemma 2, we can derive an approximated expression of the AMI as follows.

**Theorem 1.** The average mutual information achieved without CSIT can be approximated as

$$\mathcal{I}_M^{\mathcal{X}} \approx \mathcal{G} \left\langle \sum_{k=1}^{V_1} \sum_{l=1}^{V_1} \frac{w_k w_l I_M^{\mathcal{X}} \left( \frac{4U_{N_t} \bar{\gamma} t_k t_l}{m_r N_t} \right)}{\Gamma(N_r m_r) t_l^{-j} t_k^{1-N_r m_r}} \right\rangle, \quad (9)$$

where  $\{w_i\}$  and  $\{t_i\}$  denote the weight and abscissas factors of the Gauss-Laguerre integration;  $V_1$  is a complexity-accuracy tradeoff parameter.

*Proof:* The AMI can be calculated as

$$\mathcal{I}_M^{\mathcal{X}} = \int_0^\infty \left( \int_0^\infty f_G\left(\frac{x}{y}\right) \frac{f_F(y)}{y} dy \right) I_M^{\mathcal{X}}\left(\frac{x\bar{\gamma}}{N_t}\right) dx. \quad (10)$$

Using the Gauss-Laguerre quadrature rule [9, eq. (3.5.27)] to calculate the two definite integrals in (10) successively, we obtain the approximated expression shown in (9). ■

3) *Asymptotic Analysis*: We now move on to investigate the asymptotic behaviour of the AMI when the SNR approaches infinity, namely  $\bar{\gamma} \rightarrow \infty$ , which is summarized in Theorem 2.

**Theorem 2.** When  $\bar{\gamma} \rightarrow \infty$ , the AMI achieved without CSIT can be characterized as  $\mathcal{I}_M^{\mathcal{X}} \simeq \log_2 M - (\mathcal{G}_a \bar{\gamma})^{-\mathcal{G}_d}$ , where

$$\mathcal{G}_d = 1, \quad (11)$$

$$\mathcal{G}_a = \sum_{i_1=0}^{m_t-1} \cdots \sum_{i_{N_t}=0}^{m_t-1} \frac{U_{N_t}^{-S_{N_t}} S_{N_t}! Y_{N_t} \hat{\mathcal{M}}(2) m_t m_r \log_2 e}{(N_r m_r - 1) \prod_{k=1}^{N_t} \left( \frac{(i_k!)^2}{(1-m_t)_{i_k}} \right)} > 0. \quad (12)$$

Here,  $\hat{\mathcal{M}}(x) \triangleq \mathcal{M}[mmse_M^{\mathcal{X}}(t); x]$ , where  $mmse_M^{\mathcal{X}}(t)$  denotes the minimum mean square error (MMSE) in estimating  $X$  in (4) by observing  $Y$  and  $\mathcal{M}[p(t); z] \triangleq \int_0^\infty t^{z-1} p(t) dt$  denotes the Mellin transform of  $p(t)$  [11].

*Proof:* Please refer to Appendix A for more details. ■

**Remark 1.** The results in Theorem 2 suggest that the AMI achieved by finite input signals converges to its global maxi-

num,  $\log_2 M$ , as the SNR increases and its rate of convergence (ROC) equals to the rate of  $(\mathcal{G}_a \bar{\gamma})^{-\mathcal{G}_d}$  converging to 0.

**Remark 2.** For the considered channel having finite inputs, we can define its diversity order and array gain as  $\mathcal{G}_d$  and  $\mathcal{G}_a$ , respectively. Moreover, the diversity order is independent with  $N_r$  and  $N_t$ , which suggests that the deployment of multiple antennas will influence the AMI achieved without CSIT via shaping its array gain instead of its diversity order.

In the following corollary, we present the asymptotic AMI for a special case, where the amplitudes of the channel coefficients follow the Rayleigh distribution, namely  $m_t = m_r = 1$ .

**Corollary 1.** When  $\bar{\gamma} \rightarrow \infty$ , the AMI of Rayleigh keyhole channels achieved without CSIT satisfies

$$\mathcal{I}_M^{\mathcal{X}} \simeq \log_2 M - \hat{\mathcal{M}}(2) \log_2 e / (\bar{\gamma} (N_r - 1)). \quad (13)$$

**Remark 3.** From Corollary 1, we find that the array gain of Rayleigh keyhole channels achieved without CSIT is proportional to  $N_r$  but is independent of  $N_t$ . The reason lies in that an all-one precoder is adopted for randomly beamforming, whereas a matched filter is used for optimally combining.

#### B. With CSIT

When CSIT is available, the precoding vector can be designed more smartly, which is given by  $\mathbf{w} = \frac{1}{\|\mathbf{h}_t\|} \mathbf{h}_t$ . Accordingly, the AMI can be expressed as  $\mathcal{I}_M^{\mathcal{X}} = \mathbb{E} \{ I_M^{\mathcal{X}}(\bar{\gamma} S_2) \}$ , where  $S_2 = \|\mathbf{h}_r\|^2 \|\mathbf{h}_t\|^2 = \left( \sum_{i=1}^{N_r} \alpha_i^2 \right) \left( \sum_{i=1}^{N_t} \beta_i^2 \right)$ .

1) *Channel Statistics:* Using similar steps as outlined in the proof of Lemma 2, we arrive at the following lemma.

**Lemma 3.** The PDF of  $S_2$  is given by

$$f_{S_2}(x) = \frac{2(m_t m_r)^{\frac{N_t m_t + N_r m_r}{2}}}{\Gamma(N_t m_t) \Gamma(N_r m_r)} K_{N_r m_r - N_t m_t} (2\sqrt{m_t m_r x}) \times x^{\frac{N_t m_t + N_r m_r}{2} - 1}. \quad (14)$$

2) *Explicit Analysis:* The AMI achieved with CSIT can be calculated as  $\mathcal{I}_M^{\mathcal{X}} = \int_0^\infty f_{S_2}(x) I_M^{\mathcal{X}}(\bar{\gamma} x) dx$ . By the similar way as in deriving (9), we can obtain the approximated expression of AMI achieved with CSIT as follows:

$$\mathcal{I}_M^{\mathcal{X}} \approx \sum_{k=1}^{V_2} \sum_{l=1}^{V_2} \frac{w_k w_l t_j^{N_r m_r - 1} t_l^{N_t m_t - 1}}{\Gamma(N_r m_r) \Gamma(N_t m_t)} I_M^{\mathcal{X}} \left( \frac{\bar{\gamma} t_k t_l}{m_r m_t} \right), \quad (15)$$

where  $V_2$  is a complexity-accuracy tradeoff parameter.

3) *Asymptotic Analysis:* By continuously using the method detailed in Appendix A, we find that the high-SNR asymptotic AMI achieved with CSIT can be described as follows.

**Theorem 3.** When  $\bar{\gamma} \rightarrow \infty$ , the asymptotic AMI achieved with CSIT satisfies  $\mathcal{I}_M^{\mathcal{X}} \simeq \log_2 M - (\mathcal{G}_a \bar{\gamma})^{-\mathcal{G}_d}$ , where

$$\mathcal{G}_d = \min \{N_t m_t, N_r m_r\}, \quad (16)$$

$$\mathcal{G}_a = \frac{1}{m_r m_t} \left( \frac{\Gamma(N_t m_t) \Gamma(N_r m_r) \mathcal{G}_d \ln 2}{\Gamma(|N_t m_t - N_r m_r|) \hat{\mathcal{M}}(\mathcal{G}_d + 1)} \right)^{1/\mathcal{G}_d}. \quad (17)$$

Note that Theorem 3 is derived by assuming  $N_r m_r \neq N_t m_t$ . In the following, we compare the AMI achieved with CSIT with that achieved without CSIT. Furthermore, by letting  $m_t = m_r = 1$ , we arrive at the following corollary.

**Corollary 2.** When  $\bar{\gamma} \rightarrow \infty$ , the AMI of Rayleigh keyhole channels achieved with CSIT satisfies

$$\mathcal{I}_M^{\mathcal{X}} \simeq \log_2 M - \frac{\Gamma(|N_t - N_r|) \hat{\mathcal{M}}(\min\{N_t, N_r\} + 1)}{\Gamma(N_t) \Gamma(N_r) \min\{N_t, N_r\} \ln 2}. \quad (18)$$

**Remark 4.** By comparing (11) and (16), it can be observed that the diversity order achieved with CSIT is a function of  $\{N_t, N_r, m_t, m_r\}$ , which can be set larger than that achieved with no CSIT via increasing the number of antennas.

**Remark 5.** Comparing (13) with (18), we find that the array gain of Rayleigh keyhole channels achieved with CSIT is a function of  $\{N_r, N_t\}$  rather than being independent with  $N_t$ . The reason for this lies in that both optimal precoding and combining vectors can be utilized if CSIT is available.

#### IV. EXTENSION TO MULTI-STREAM TRANSMISSION

Having characterized the SS-AMI, we now move on to discuss the AMI under multi-stream transmission (MS-AMI). In this case, the received signal vector satisfies

$$\mathbf{y} = \sqrt{\bar{\gamma}} \mathbf{H} \mathbf{P} \mathbf{x} + \mathbf{n}, \quad (19)$$

where  $\mathbf{x} = [x_1, \dots, x_L] \in \mathbb{C}^{L \times 1}$  denotes the data vector with i.i.d. elements drawn from an equiprobable  $M$ -ary constellation,  $\mathcal{S}$ ;  $\mathbb{E} \{\mathbf{x} \mathbf{x}^H\} = \mathbf{I}_L$  with  $L$  being the number of data streams; and  $\mathbf{P} \in \mathbb{C}^{N_t \times L}$  denotes the precoding matrix subject to  $\text{tr} \{\mathbf{P} \mathbf{P}^H\} = 1$ . Accordingly, the MI can be written as  $I(\bar{\gamma}; \mathbf{H} \mathbf{P}) = L \log_2 M - N_r \log_2 e - M^{-L} f(\bar{\gamma}; \mathbf{H} \mathbf{P})$  [7], where  $f(\bar{\gamma}; \mathbf{H} \mathbf{P}) \triangleq \sum_{i=1}^{M^L} \mathbb{E}_{\mathbf{n}} \left\{ \log_2 \left( \sum_{j=1}^{M^L} e^{-\|\mathbf{n} + \sqrt{\bar{\gamma}} \mathbf{H} \mathbf{P} \mathbf{e}_{ij}\|^2} \right) \right\}$  with  $\mathbf{e}_{ij} \triangleq \mathbf{x}_i - \mathbf{x}_j = [e_{i,j,1}, \dots, e_{i,j,L}]^T$  and  $\mathbf{x}_i = [x_{i,1}, \dots, x_{i,L}]^T$  being a realization of  $\mathbf{x}$  with  $x_{i,j} \in \mathcal{S}$ .

##### A. Without CSIT

We first consider the case of no CSIT and the precoding matrix is  $\mathbf{P} = 1/\sqrt{N_t} \mathbf{I}_{N_t} \triangleq \mathbf{P}_{\text{no}}$ . Unfortunately, it is challenging to derive any closed-form expressions of  $\mathcal{I}_M^{\mathcal{S}} \triangleq \mathbb{E} \{ I(\bar{\gamma}; \mathbf{H} \mathbf{P}_{\text{no}}) \}$ . Hence, we will pay more attention to the high-SNR AMI.

**Theorem 4.** When  $\bar{\gamma} \rightarrow \infty$ , the AMI achieved without CSIT can be characterized as  $\mathcal{I}_M^{\mathcal{S}} \simeq N_t \log_2 M - \mathcal{O}(\bar{\gamma}^{-1})$ .

*Proof:* Please refer to Appendix B for more details. ■

**Remark 6.** The results in Theorem 4 suggest that the diversity order of the multi-stream AMI achieved without CSIT is given by  $\mathcal{G}_d = 1$ , which is the same as that of single-stream AMI. Besides, we comment that the array gain of  $\mathcal{I}_M^{\mathcal{S}}$  is sandwiched between its lower and upper bounds derived in Appendix B.

##### B. With CSIT

Turn now to the case with CSIT. Yet, it is hard to get a closed-form expression of  $\mathbf{P}$  that can maximize  $I(\bar{\gamma}; \mathbf{H} \mathbf{P})$  [12].

1) *MRT Precoding:* As a compromise, we first analyze the AMI achieved by the MRT precoding. Then, we have  $\mathbf{P} = [\text{tr}(\mathbf{H}^H \mathbf{H})]^{-1/2} \mathbf{H}^H \triangleq \mathbf{P}_{\text{mrt}}$ , which yields  $\mathbf{y} = \sqrt{\bar{\gamma}} \mathbf{G} \mathbf{x} + \mathbf{n}$  with  $\mathbf{G} = \|\mathbf{h}_t\| \frac{\mathbf{h}_r}{\|\mathbf{h}_r\|} \mathbf{h}_t^H$ . Following a similar approach as that in Appendix B, we arrive at the following results.

**Theorem 5.** When  $\bar{\gamma} \rightarrow \infty$ , the AMI achieved by the MRT precoding can be characterized as  $\mathcal{I}_M^{\mathcal{S}} \simeq N_r \log_2 M - \mathcal{O}(\bar{\gamma}^{-1})$ .

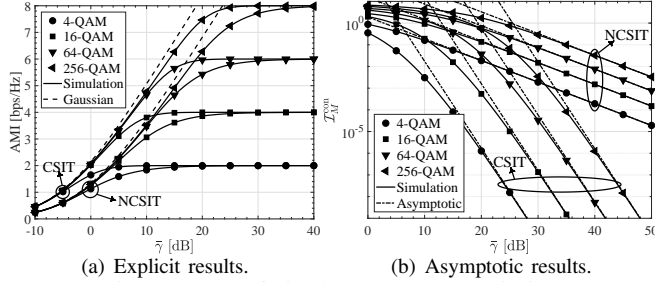


Fig. 2: AMI of single-stream transmission.

It is worth noting that the diversity order achieved by the MRT precoding is  $\mathcal{G}_d = 1$ , which is the same as that achieved without CSIT. Due to this, we proceed to another precoding scheme that is capable of improving the diversity order.

2) *Max- $d_{\min}$  Precoding*: In fact, the optimization of  $I(\bar{\gamma}; \mathbf{H}\mathbf{P})$  at the high-SNR region is equivalent to maximizing the minimum distance  $d_{\min} \triangleq \min_{i \neq j} \|\mathbf{H}\mathbf{P}\mathbf{e}_{i,j}\| = \min_{i \neq j} |\mathbf{h}_i^H \mathbf{P}\mathbf{e}_{i,j}|$  [12]. Motivated by this, we move on to discuss the AMI achieved by a heuristic precoder  $\mathbf{P} = \frac{1}{\|\mathbf{h}\|} \mathbf{h} \mathbf{d}_*^H \triangleq \mathbf{P}_{mm}$  with  $\mathbf{d}_* = \arg \max_{\|\mathbf{x}\|=1} \min_{i \neq j} |\mathbf{x}^H \mathbf{e}_{i,j}|$ . Note that  $\mathbf{d}_*$  can be obtained via an exhaustive search since it is independent of  $\mathbf{H}$ . Leveraging (14) and following a similar approach as that in Appendix B, we obtain Theorem 6.

**Theorem 6.** When  $\bar{\gamma} \rightarrow \infty$ , the AMI achieved by the Max- $d_{\min}$  precoding can be characterized as  $\mathcal{I}_M^S \simeq L \log_2 M - \mathcal{O}(\bar{\gamma}^{-\mathcal{G}_d})$  with  $\mathcal{G}_d = \min\{N_t m_t, N_r m_r\}$ .

**Remark 7.** In contrast to  $\mathbf{P}_{no}$  and  $\mathbf{P}_{mrt}$ , the diversity order achieved by  $\mathbf{P}_{mm}$  can be improved by increasing  $N_r$  and  $N_t$ , which highlights the superiority of the Max- $d_{\min}$  precoder.

## V. NUMERICAL RESULTS

The rationality of previous analyses are validated via numerical results in this part where we set  $N_t = N_r = 2$ ,  $m_t = 2$ , and  $m_r = 3$ . Fig. 2(a) plots the SS-AMI achieved by  $M$ -QAM signals ( $M = 4, 16, 64, 256$ ), where the approximated AMI (denoted by symbols) is calculated by (9) or (15) via setting  $V_1 = 200$ . As can be seen, the approximated results fit well with the simulated results and the AMI achieved with CSIT is higher than that achieved without CSIT. For comparison, we also plot the AMI achieved by Gaussian signaling in Fig. 2(a). As shown, the AMI of Gaussian inputs increases without bound as  $\bar{\gamma}$  increases, whereas the AMI of finite inputs converges to  $\log_2 M$ , in the large limit of  $\bar{\gamma}$ . By Remark 1, the rate of the AMI ( $\mathcal{I}_M^X$ ) converging to  $\log_2 M$  equals the rate of  $\mathcal{I}_M^{\text{con}} = \log_2 M - \mathcal{I}_M^X$  converging to zero. To illustrate the ROC, we plot  $\mathcal{I}_M^{\text{con}}$  versus  $\bar{\gamma}$  in Fig. 2(b). As shown, the derived asymptotic results track the numerical results accurately in the high-SNR regime. Moreover, it can be seen that the AMI achieved with CSIT yields a faster ROC (or a higher diversity order) than that achieved without CSIT, which is consistent with the conclusion in Remark 4.

Fig. 3(a) compares the MS-AMI and SS-AMI achieved by 4-QAM and Gaussian signals. As shown, in both cases with and without CSIT, the MS-AMI is higher than the SS-AMI and the Gaussian signals achieve higher AMI than finite-input signals. Moreover, it is observed that the Max- $d_{\min}$  precoder yields virtually the same AMI as the MRT precoder but

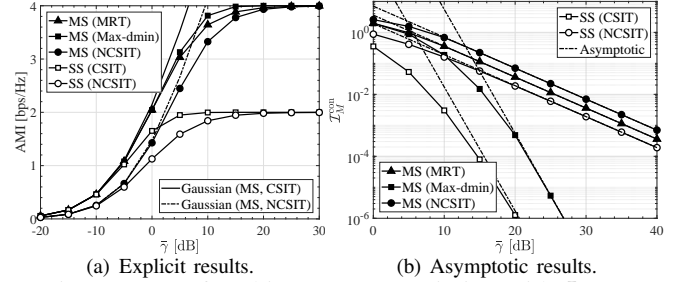


Fig. 3: AMI of multi-stream transmission with  $L = 2$ .

outperforms the latter one in the high-SNR regime. Fig. 3(b) plots  $\mathcal{I}_M^{\text{con}} = \log_2 M - \mathcal{I}_M^X$  (for SS) and  $\mathcal{I}_M^{\text{con}} = L \log_2 M - \mathcal{I}_M^S$  (for MS) versus  $\bar{\gamma}$  to show the ROC of the AMI. Notably, the diversity order of the MS-AMI is obtained in Section IV, whereas the corresponding array gain is unknown. As a compromise, the asymptotic curve for the MS-AMI is obtained by moving the curve of  $\bar{\gamma}^{-\mathcal{G}_d}$  in the coordinate plane so as to track the corresponding AMI curve in the high-SNR region. As shown, the obtained asymptotic curves can track the high-SNR curves of  $\mathcal{I}_M^{\text{con}}$  well, which supports the asymptotic analyses in Section IV. Moreover, Fig. 3(b) suggests that the AMI achieved by the Max- $d_{\min}$  precoder yields a faster ROC (or a higher diversity order) than the MRT precoder, which is consistent with the conclusion in Remark 7.

## VI. CONCLUSION

The AMI of keyhole MIMO channels having finite inputs was investigated under both single-stream and multi-stream transmission. Theoretical analyses indicated that the ROC of the AMI is determined by the array gain and the diversity order, which can be accelerated by properly using the CSIT.

## APPENDIX A PROOF OF THEOREM 2

*Proof:* To facilitate the derivation, we rewrite the AMI as

$$\begin{aligned} \dot{\mathcal{I}}_M^X &= I_M^X(t) F_{S_1} \left( \frac{N_t t}{\bar{\gamma}} \right) \Big|_0^\infty - \int_0^\infty F_{S_1} \left( \frac{N_t t}{\bar{\gamma}} \right) dI_M^X(t) \\ &= \log_2 M - \int_0^\infty \int_0^\infty f_{S_1}(x) dx \frac{\text{mmse}_M^X(t)}{\ln 2} dt, \quad (20) \end{aligned}$$

where  $F_{S_1}(\cdot)$  denotes the cumulative distribution function (CDF) of  $S_1$  and  $\text{mmse}_M^X(\gamma) = \frac{1}{\log_2 e} \frac{dI_M^X(\gamma)}{d\gamma}$  is the MMSE in estimating  $X$  in (4) by observing  $Y$  [13]. When  $\bar{\gamma} \rightarrow \infty$ , we obtain  $\frac{1}{\bar{\gamma}} \rightarrow 0$ , which together with (20) and the facts of  $K_\nu(z) = \bar{K}_{-\nu}(z)$  [9, eq. (10.27.3)] and  $\lim_{z \rightarrow 0} K_\nu(z) = \frac{1}{2} \Gamma(\nu) (\frac{1}{2} z)^{-\nu}$  ( $\nu > 0$ ) [9, eq. (10.30.2)], yields

$$\dot{\mathcal{I}}_M^X \simeq \log_2 M - \mathcal{G} \left\langle \frac{\Gamma(|N_r m_r - j - 1|) \hat{\mathcal{M}}(\bar{j} + 1)}{\Gamma(N_r m_r) \bar{j} (4U_{N_r} \bar{\gamma} / (N_r m_r))^{\bar{j}} \ln 2} \right\rangle. \quad (21)$$

Here,  $\bar{j} \triangleq \min\{N_r m_r, j + 1\}$  and  $\hat{\mathcal{M}}(x) = \mathcal{M}[\text{mmse}_M^X(t); x]$ , where  $\mathcal{M}[p(t); z] = \int_0^\infty t^{z-1} p(t) dt$  denotes the Mellin transform of  $p(t)$  [11]. It is worthy of mentioning that in obtaining (21), we assumed  $N_r m_r - j - 1 \neq 0$  ( $\forall j$ ) for simplicity. Then, we introduce the following two lemmas for further discussion.

**Lemma 4.** If the constellation alphabet  $\mathcal{X} = \{x_i\}_{i=1}^M$  has no accumulation point, namely  $d_{\mathcal{X},\min} \triangleq \inf_{i \neq j} |x_i - x_j| > 0$ , then it has  $\text{mmse}_{\mathcal{M}}^{\mathcal{X}}(\gamma) \leq \mathcal{O}\left(\gamma^{-\frac{1}{2}} e^{-\frac{\gamma}{8} d_{\mathcal{X},\min}^2}\right)$  [14].

**Lemma 5.** If  $p(t)$  is  $\mathcal{O}(t^a)$  as  $t \rightarrow 0^+$  and  $\mathcal{O}(t^b)$  as  $t \rightarrow +\infty$ , then  $|\mathcal{M}[p(t); z]| < \infty$  when  $-a < z < -b$  [11].

In this letter, we focus more on the constellation alphabet used in practical systems, for example  $M$ -QAM, and the condition of  $d_{\mathcal{X},\min} = \inf_{i \neq j} |x_i - x_j| > 0$  is satisfied. Hence, Lemma 4 can be directly used. By [13],  $\lim_{t \rightarrow 0^+} \text{mmse}_{\mathcal{M}}^{\mathcal{X}}(t) = 1$ , which together with Lemma 4 shows,  $\text{mmse}_{\mathcal{M}}^{\mathcal{X}}(t)$  is  $\mathcal{O}(t^0)$  as  $t \rightarrow 0^+$  and  $\mathcal{O}(t^{-\infty})$  as  $t \rightarrow \infty$ . Using this fact and Lemma 5, we find that  $|\hat{\mathcal{M}}(x)| < \infty$  holds for  $0 < x < \infty$ , which in combination with the fact that  $\text{mmse}_{\mathcal{M}}^{\mathcal{X}}(x) > 0$  ( $x > 0$ ) [13], suggests that  $\hat{\mathcal{M}}(x) \in (0, \infty)$  holds for  $0 < x < \infty$ . It follows from  $\bar{j} = \min\{N_r m_r, j+1\} > 0$  that  $\hat{\mathcal{M}}(\bar{j}+1) \in (0, \infty)$ . As previously assumed,  $N_r > 1$  and  $m_r$  takes integers, which yields  $N_r m_r > 1$ . We then neglect the higher order terms in (21) to derive the asymptotic AMI as  $\hat{\mathcal{I}}_{\mathcal{M}}^{\mathcal{X}} \simeq \log_2 M - \Psi \bar{\gamma}^{-\Phi}$ , where  $\Phi = 1$  and  $\Psi = \sum_{i_1=0}^{m_t-1} \dots \sum_{i_{N_t}=0}^{m_t-1} \frac{U_{N_t}^{-S_{N_t}} S_{N_t}! Y_{N_t} \hat{\mathcal{M}}(2)^{m_t m_r} \log_2 e}{(N_r m_r - 1) \prod_{k=1}^{N_t} \left( \frac{(i_k!)^2}{(1-m_t)_{i_k}} \right)}$ . Furthermore, since  $F_{S_1}(x) > 0$  and  $\text{mmse}_{\mathcal{M}}^{\mathcal{X}}(x) > 0$  ( $x > 0$ ),  $\Psi \bar{\gamma}^{-\Phi} = \lim_{\bar{\gamma} \rightarrow \infty} \int_0^\infty F_{S_1}\left(\frac{N_t t}{\bar{\gamma}}\right) \text{mmse}_{\mathcal{M}}^{\mathcal{X}}(t) dt > 0$  holds, which suggests that  $\Psi > 0$  and thus  $\Psi^{-\frac{1}{\Phi}} > 0$ . ■

#### APPENDIX B PROOF OF THEOREM 4

*Proof:* The MI satisfies  $I(\bar{\gamma}; \mathbf{HP}) = L \log_2 M - \frac{1}{\ln 2} \int_{\bar{\gamma}}^\infty \text{mmse}_{\mathcal{M}}^{\mathcal{X}}(x; \mathbf{HP}) dx$  [12], where  $\text{mmse}_{\mathcal{M}}^{\mathcal{X}}(\bar{\gamma}; \mathbf{HP})$  denotes the MMSE of (19) in estimating  $\mathbf{x}$  by observing  $\mathbf{y}$ . Moreover, for any MIMO channels, the MMSE is bounded by  $\underline{\text{mmse}}_{\mathcal{M}}^{\mathcal{X}}(\bar{\gamma}; \mathbf{HP}) \leq \text{mmse}_{\mathcal{M}}^{\mathcal{X}}(\bar{\gamma}; \mathbf{HP}) \leq \overline{\text{mmse}}_{\mathcal{M}}^{\mathcal{X}}(\bar{\gamma}; \mathbf{HP})$  [12]. Defining  $f_l(x) \triangleq 1 - \frac{1}{\sqrt{\pi}} \int_{-\infty}^{+\infty} \tanh(\sqrt{x}a) e^{-(a - \frac{\sqrt{x}}{2})^2} da$ ,  $f_u(x) \triangleq Q(\sqrt{\frac{x}{2}})$  with  $Q(x) \triangleq \frac{1}{\sqrt{2\pi}} \int_x^\infty e^{-u^2/2} du$  being the Q-function, and  $d_{i,j} \triangleq \|\mathbf{HPe}_{i,j}\|^2$ , we have [12, Appendix III]

$$\underline{\text{mmse}}_{\mathcal{M}}^{\mathcal{X}}(\bar{\gamma}; \mathbf{HP}) = \sum_{i,j=1,j \neq i}^{M^L} \frac{d_{i,j}}{4M^L} \frac{f_l(\bar{\gamma} d_{i,j})}{M^L - 1}, \quad (22)$$

$$\overline{\text{mmse}}_{\mathcal{M}}^{\mathcal{X}}(\bar{\gamma}; \mathbf{HP}) = \sum_{i,j=1,j \neq i}^{M^L} \frac{d_{i,j}}{M^L} f_u(\bar{\gamma} d_{i,j}). \quad (23)$$

Therefore, the AMI is upper bounded by

$$\mathcal{I}_{\mathcal{M}}^{\mathcal{X}} \leq L \log_2 M - \frac{1}{\ln 2} \int_{\bar{\gamma}}^\infty \underline{\text{mmse}}_{\mathcal{M}}^{\mathcal{X}}(x; \mathbf{HP}) dx \quad (24a)$$

$$= L \log_2 M - \sum_{i,j=1,j \neq i}^{M^L} \frac{\mathcal{I}_{\mathcal{M},i,j}^{\mathcal{X}} \log_2 e}{4(M^L - 1)M^L} \triangleq \overline{\mathcal{I}}_{\mathcal{M}}^{\mathcal{X}}, \quad (24b)$$

where  $\mathcal{I}_{\mathcal{M},i,j}^{\mathcal{X}} \triangleq \int_0^\infty \int_{\bar{\gamma}}^\infty y f_l(\bar{\gamma} y) f_{i,j}(y) dx dy$  with  $f_{i,j}(y)$  denoting the PDF of  $d_{i,j}$ . It follows that  $\mathcal{I}_{\mathcal{M},i,j}^{\mathcal{X}} = \int_0^\infty \frac{1}{\bar{\gamma}} f_{i,j}\left(\frac{y}{\bar{\gamma}}\right) \int_y^\infty f_l(x) dx dy$ . When  $\mathbf{P} = 1/\sqrt{N_t} \mathbf{I}_{N_t}$ , we have  $d_{i,j} = \|\mathbf{h}_i\|^2 |1/\sqrt{N_t} \mathbf{h}_i^H \mathbf{e}_{i,j}|^2$ , whose PDF presents the same form as (8) by setting  $Y_{N_t} = \prod_{k=1}^{N_t} \left( \frac{|e_{i,j,k}|}{4m_t N_t} \right)^{i_k}$  and

$U_{N_t} = \sum_{k=1}^{N_t} \frac{|e_{i,j,k}|}{4m_t N_t}$ . Following similar steps as in Appendix A, we find that when  $\bar{\gamma} \rightarrow \infty$ ,

$$\mathcal{I}_{\mathcal{M},i,j}^{\mathcal{X}} \simeq \sum_{i_1=0}^{m_t-1} \dots \sum_{i_{N_t}=0}^{m_t-1} \frac{S_{N_t}! Y_{N_t} m_r \hat{\mathcal{M}}_l(1) U_{N_t}^{-S_{N_t}-1} \bar{\gamma}^{-1}}{4(N_r m_r - 1) \prod_{k=1}^{N_t} \left( \frac{(i_k!)^2}{(1-m_t)_{i_k}} \right)}, \quad (25)$$

where  $\mathcal{M}_l(t) \triangleq \mathcal{M}\left[\int_y^\infty f_l(x) dx; t\right]$ . Define  $\underline{f}(y) = \int_y^\infty f_l(x) dx$ . We find  $\lim_{x \rightarrow 0^+} f_l(x) = 0$  and  $\lim_{x \rightarrow \infty} f_l(x) = \mathcal{O}\left(e^{-\frac{x}{2}} x^{-\frac{1}{2}}\right)$  [13, Theorem 3, Appendix B], which suggests that  $f_l(x)$  is  $\mathcal{O}(x^a)$  ( $a \geq 0$ ) as  $t \rightarrow 0^+$  and  $\mathcal{O}(x^{-\infty})$  as  $x \rightarrow \infty$ . It follows from this fact and Lemma 5 that  $\lim_{y \rightarrow 0^+} \underline{f}(y) = \int_0^\infty f_l(x) dx = \mathcal{O}(y^0) \in (0, \infty)$ . Moreover, using the L'Hôpital's rule and [13, Appendix B] yields  $\lim_{y \rightarrow \infty} \underline{f}(y) = \mathcal{O}\left(e^{-\frac{x}{2}} x^{-\frac{1}{2}}\right)$ . By continuously using Lemma 5, we can conclude that  $\mathcal{M}_l(1) \in (0, \infty)$ , which in combination with (24) and (25), indicates

$$\lim_{\bar{\gamma} \rightarrow \infty} \mathcal{I}_{\mathcal{M}}^{\mathcal{X}} \leq \lim_{\bar{\gamma} \rightarrow \infty} \overline{\mathcal{I}}_{\mathcal{M}}^{\mathcal{X}} = N_t \log_2 M - \mathcal{O}(\bar{\gamma}^{-1}). \quad (26)$$

Turn now to the AMI's lower bound given by  $\mathcal{I}_{\mathcal{M}}^{\mathcal{X}} \geq L \log_2 M - \sum_{i,j=1,j \neq i}^{M^L} \frac{\mathcal{I}_{\mathcal{M},i,j}^{\mathcal{X}}}{M^L \ln 2} \triangleq \underline{\mathcal{I}}_{\mathcal{M}}^{\mathcal{X}}$  with  $\overline{\mathcal{I}}_{\mathcal{M},i,j}^{\mathcal{X}} \triangleq \int_0^\infty \int_{\bar{\gamma}}^\infty y f_u(\bar{\gamma} y) f_{i,j}(y) dx dy$ . By following a similar way in deriving (26), we can prove  $\lim_{\bar{\gamma} \rightarrow \infty} \mathcal{I}_{\mathcal{M}}^{\mathcal{X}} \geq \lim_{\bar{\gamma} \rightarrow \infty} \underline{\mathcal{I}}_{\mathcal{M}}^{\mathcal{X}} = N_t \log_2 M - \mathcal{O}(\bar{\gamma}^{-1})$ , which together with (26), yields  $\lim_{\bar{\gamma} \rightarrow \infty} \mathcal{I}_{\mathcal{M}}^{\mathcal{X}} = N_t \log_2 M - \mathcal{O}(\bar{\gamma}^{-1})$ . ■

#### REFERENCES

- [1] D. Chizhik, *et al.*, "Keyholes, correlations, and capacities of multielement transmit and receive antennas," *IEEE Trans. Wireless Commun.*, vol. 1, no. 2, pp. 361–368, Apr. 2002.
- [2] H. Shin and J. H. Lee, "Capacity of multiple-antenna fading channels: Spatial fading correlation, double scattering, and keyhole," *IEEE Trans. Inf. Theory*, vol. 49, no. 10, pp. 2636–2647, Oct. 2003.
- [3] A. Maaref, *et al.*, "Impact of spatial fading correlation and keyhole on the capacity of MIMO systems with transmitter and receiver CSI," *IEEE Trans. Wireless Commun.*, vol. 7, no. 8, pp. 3218–3229, Aug. 2008.
- [4] P. Almers, *et al.*, "Keyhole effect in MIMO wireless channels: Measurements and theory," *IEEE Trans. Wireless Commun.*, vol. 5, no. 12, pp. 3596–3604, Dec. 2006.
- [5] A. Müller, *et al.*, "Ergodic capacity and information outage probability of MIMO Nakagami- $m$  keyhole channels with general branch parameters," in *Proc. IEEE WCNC*, Mar. 2007, pp. 2184–2189.
- [6] P. Almers, *et al.*, "Measurement of keyhole effect in a wireless multiple-input multiple-output (MIMO) channel," in *IEEE Commun. Lett.*, vol. 7, no. 8, pp. 373–375, Aug. 2003.
- [7] R. W. Heath, Jr., and A. Lozano, *Foundation MIMO Communication*, Cambridge, U.K.: Cambridge Univ. Press, 2018.
- [8] I. S. Gradshteyn and I. M. Ryzhik, *Table of Integrals, Series and Products*, 7th ed., Academic, San Diego, C.A., 2007.
- [9] R. B. Paris, *NIST Handbook of Mathematical Functions*, Cambridge, U.K.: Cambridge Univ. Press, 2010.
- [10] G. K. Karagiannidis, "A closed-form solution for the distribution of the sum of Nakagami- $m$  random phase vectors," *IEEE Commun. Lett.*, vol. 10, no. 12, pp. 828–830, Dec. 2006.
- [11] P. Flajolet, *et al.*, "Mellin transforms and asymptotics: Harmonic sums," *Theoretical Computer Science*, vol. 144, no. 1–2, pp. 3–58, 1995.
- [12] F. Pérez-Cruz, M. R. D. Rodrigues, and S. Verdú, "MIMO Gaussian channels with arbitrary inputs: Optimal precoding and power allocation," *IEEE Trans. Inf. Theory*, vol. 56, no. 3, pp. 1070–1084, Mar. 2010.
- [13] A. Lozano, A. M. Tulino, and S. Verdú, "Optimum power allocation for parallel Gaussian channels with arbitrary input distributions," *IEEE Trans. Inf. Theory*, vol. 52, no. 7, pp. 3033–3051, Jul. 2006.
- [14] Y. Wu and S. Verdú, "MMSE dimension," *IEEE Trans. Inf. Theory*, vol. 57, no. 8, pp. 4857–4879, Aug. 2011.